Article:
Lhardy, F, Bouttes, N, Roche, DM et al. (15 more authors) (2021) A First Intercomparison of the Simulated LGM Carbon Results Within PMIP-Carbon: Role of the Ocean Boundary Conditions. Paleoceanography and Paleoclimatology, 36 (10). e2021PA004302. ISSN 2572-4525

https://doi.org/10.1029/2021pa004302

A first intercomparison of the simulated LGM carbon results within PMIP-carbon: role of the ocean boundary conditions

F. Lhardy[1], N. Bouttes[1], D. M. Roche[1,2], A. Abe-Ouchi[3], Z. Chase[4], K. A. Crichton[5], T. Ilyina[6], R. Ivanovic[7], M. Jochum[8], M. Kageyama[1], H. Kobayashi[3], B. Liu[6], L. Menviel[9], J. Muglia[10], R. Nuterman[8], A. Oka[3], G. Vettoretti[8], A. Yamamoto[11]

[1]Laboratoire des Sciences du Climat et de l'Environnement, CEA-CNRS-UVSQ, Gif-sur-Yvette, France
[2]Vrije Universiteit Amsterdam, Faculty of Science, Department of Earth Sciences, Earth and Climate cluster, Amsterdam, The Netherlands
[3]Atmosphere and Ocean Research Institute, The University of Tokyo, Kashiwa, Japan
[4]University of Tasmania, Hobart, Australia
[5]School of Geography, Exeter University, Exeter, UK
[6]Max Planck Institute for Meteorology, Hamburg, Germany
[7]University of Leeds, Leeds, UK
[8]Niels Bohr Institute, University of Copenhagen, Copenhagen, Denmark
[9]Climate Change Research Centre, the University of New South Wales, Sydney, Australia
[10]Centro para el Estudio de los Sistemas Marinos, CONICET, 2915 Boulevard Brown, U9120ACD, Puerto Madryn, Argentina
[11]Japan Agency for Marine-Earth Science and Technology, Yokohama, Japan

Key Points:

- Ocean volume is a dominant control on LGM carbon sequestration and must be accurately represented in models.
- Adjusting the alkalinity to account for the relative change of volume at the LGM induces a large increase of oceanic carbon (of ~ 250 GtC).
- PMIP-carbon models standardly simulate high LGM CO_2 levels (over 300 ppm) despite a larger proportion of carbon in the ocean at LGM than PI.

Corresponding author: Fanny Lhardy, fanny.lhardy@lsce.ipsl.fr

Abstract

Model intercomparison studies of coupled carbon-climate simulations have the potential to improve our understanding of the processes explaining the pCO_2 drawdown at the Last Glacial Maximum (LGM) and to identify related model biases. Models participating in the Paleoclimate Modelling Intercomparison Project (PMIP) now frequently include the carbon cycle. The ongoing PMIP-carbon project provides the first opportunity to conduct multimodel comparisons of simulated carbon content for the LGM time window. However, such a study remains challenging due to differing implementation of ocean boundary conditions (e.g. bathymetry and coastlines reflecting the low sea level) and to various associated adjustments of biogeochemical variables (i.e. alkalinity, nutrients, dissolved inorganic carbon). After assessing the ocean volume of PMIP models at the pre-industrial and LGM, we investigate the impact of these modelling choices on the simulated carbon at the global scale, using both PMIP-carbon model outputs and sensitivity tests with the iLOVECLIM model. We show that the carbon distribution in reservoirs is significantly affected by the choice of ocean boundary conditions in iLOVECLIM. In particular, our simulations demonstrate a $\sim$ 250 GtC effect of an alkalinity adjustment on carbon sequestration in the ocean. Finally, we observe that PMIP-carbon models with a freely evolving CO_2 and no additional glacial mechanisms do not simulate the pCO_2 drawdown at the LGM (with concentrations as high as 313, 331 and 315 ppm), especially if they use a low ocean volume. Our findings suggest that great care should be taken on accounting for large bathymetry changes in models including the carbon cycle.

1 Introduction

The mechanisms of the atmospheric CO_2 variations at the scale of glacial-interglacial cycles are not fully understood. Ice core records have shown CO_2 variations with an amplitude of about 100 ppm for the last four or five cycles (Lüthi et al., 2008). In particular, the atmospheric CO_2 is known to have reached concentrations as low as 190 ppm (Bereiter et al., 2015) at 23−19 kaBP, during the Last Glacial Maximum (LGM). Compared to pre-industrial (PI) levels of around 280 ppm, this LGM pCO_2 drawdown is commonly thought to be mainly linked to an increase in carbon sequestration in the ocean (Anderson et al., 2019).

The total carbon content of this large reservoir currently holding $\sim$ 38,000 GtC (Sigman & Boyle, 2000) is influenced by both physical and biogeochemical processes (Bopp et al., 2003; Kohfeld & Ridgwell, 2009; Sigman et al., 2010; Ödalen et al., 2018). Physical processes include changes in the solubility pump: a glacial cooling is associated with higher CO_2 solubility, though counteracted by the effect of an increased salinity. They also encompass changes of Southern Ocean sea ice (Stephens & Keeling, 2000; Marzocchi & Jansen, 2019), ocean stratification (Francois et al., 1997) and circulation (Aldama-Campino et al., 2020; Ödalen et al., 2018; Watson et al., 2015; Skinner, 2009; Menviel et al., 2017; Schmittner & Galbraith, 2008). Biogeochemical processes rely on changes in the $CaCO_3$ cycle (Kobayashi & Oka, 2018; Matsumoto & Sarmiento, 2002; Brovkin et al., 2007, 2012) or an increased efficiency of the biological pump (Morée et al., 2021), through increased iron inputs from aeolian dust for example (Bopp et al., 2003; Tagliabue et al., 2009, 2014; Oka et al., 2011; Yamamoto et al., 2019).

Despite the identification of these processes, their contribution to the pCO_2 drawdown is still much debated. Modelling studies tend to show a large effect of the biological pump and a moderate effect of circulation changes (Khatiwala et al., 2019; Buchanan et al., 2016; Yamamoto et al., 2019; Tagliabue et al., 2009; Hain et al., 2010; Menviel et al., 2012), but model disagreements remain. Iron fertilization seems to explain a relatively small part ($\sim$ 15 ppm) of the LGM pCO_2 drawdown (Bopp et al., 2003; Tagliabue et al., 2014; Kohfeld & Ridgwell, 2009; Muglia et al., 2017). Accounting for carbonate compensation in models also seems to significantly reduce the simulated atmospheric CO_2 concentrations (Kobayashi & Oka, 2018; Brovkin et al., 2007). However,

review studies show that the amplitude of the CO_2 variation caused by each process is not well constrained (Kohfeld & Ridgwell, 2009; Gottschalk et al., 2020). Moreover, sensitivity tests underline that, due to the interactions of both these physical and biogeochemical processes, isolating their effect remains challenging (Hain et al., 2010; Kobayashi & Oka, 2018; Ödalen et al., 2018). The emerging common view is that the LGM pCO_2 drawdown cannot be explained by a single mechanism, but by a combination of different intrinsic processes (Kohfeld & Ridgwell, 2009; Hain et al., 2010). Gaining a better understanding of these mechanisms, which depend on the background climate, is critical to accurately project future climate (Yamamoto et al., 2018).

As a result, it is hardly surprising that models struggle to simulate the LGM pCO_2 drawdown, especially in their standard version. Previous studies show that models simulate a large range of pCO_2 drawdown, with most modelling studies accounting for one third to two thirds of the 90−100 ppm change inferred from ice core data (Brovkin et al., 2007, 2012; Buchanan et al., 2016; Matsumoto & Sarmiento, 2002; Hain et al., 2010; Khatiwala et al., 2019; Marzocchi & Jansen, 2019; Stephens & Keeling, 2000; Oka et al., 2011; Kobayashi & Oka, 2018; Tagliabue et al., 2009; Morée et al., 2021). The discrepancies between models can be partly linked to resolution (Gottschalk et al., 2020) and representation of ocean and atmosphere physics, completeness of the carbon cycle model (including sediments, permafrost...) (Kohfeld & Ridgwell, 2009), and simulated climate and ocean circulation (Menviel et al., 2017; Ödalen et al., 2018). Ödalen et al. (2018) also highlights that differences in the initial equilibrium states (which depend on the model tuning strategy at the PI) may lead to different pCO_2 drawdown potentials in models. In this context, we could learn a lot from a multimodel comparison study of standardized LGM experiments. Such studies are now common for modern and future climates: the Coupled Climate Carbon Cycle Model Intercomparison Project (C4MIP, Jones et al. (2016)) aims to quantify climate-carbon interactions in General Circulation Models (GCMs). Since the LGM is a benchmark period of the Paleoclimate Modelling Intercomparison Project (PMIP, Kageyama et al. (2018)), the stage is set for a similar study focussed on the LGM. Indeed, the PMIP project is now in its phase 4 and a standardized experimental protocol has been designed for the LGM (Kageyama et al., 2017). Although more and more PMIP models now also simulate the carbon cycle, outputs describing the carbon cycle have not been shared through ESGF (Earth System Grid Federation) systematically and no systematic multimodel analysis of coupled climate-carbon LGM experiments has been done so far. The purpose of the new PMIP-carbon project is therefore to compare outputs of various models in order to better understand the mechanisms behind past carbon cycle changes. As a first step, the project focusses on the model response to LGM conditions.

In this study, the preliminary results of the PMIP-carbon project gives us the opportunity to examine LGM carbon outputs of a roughly consistent model ensemble for the first time. We evaluate the impact of modelling choices related to the ocean boundary conditions change on the simulated carbon. We assess specifically the impacts of the total ocean volume change and associated adjustments, two elements which are not the focus of the PMIP protocol. Since the PMIP-carbon project is ongoing, this first look is especially useful to draw a few conclusions which will help refine the PMIP-carbon protocol.

2 Modelling choices in PMIP-carbon models and resulting ocean volumes

2.1 The PMIP-carbon protocol

The PMIP-carbon project, which falls under the auspices of the 'Deglaciations' working group in the PMIP structure, aims at the first multimodel comparison of coupled climate-carbon experiments at the LGM. Participating modelling groups ran both a PI and a LGM simulation with the same code, following the PMIP4 experimental design as far

as possible, but model outputs obtained using the PMIP2 or PMIP3 protocol were also accepted. These standardized protocols specify modified forcing parameters (greenhouse gas concentrations and orbital parameters) and different boundary conditions (e.g. elevation, land ice extent, coastlines, and bathymetry). Indeed, the LGM was a cold period with extensive ice sheets over the Northern Hemisphere. Due to the quantity of ice trapped on land, the eustatic sea level was around -134 m below its present value (Lambeck et al., 2014). To account for the related changes of topography (which encompasses changes of elevation, albedo, coastlines and bathymetry) in models, Kageyama et al. (2017) define the PMIP4 protocol and provide guidelines on how to implement the LGM boundary conditions on the atmosphere and ocean grids. Given the uncertainty of ice sheet reconstructions, the PMIP4 protocol lets modelling groups choose from three different topographies: GLAC-1D (Ivanovic et al., 2016), ICE-6G-C (Peltier et al., 2015; Argus et al., 2014), or PMIP3 (Abe-Ouchi et al., 2015), whereas the PMIP3 protocol relied on the PMIP3 ice sheet reconstructions (`https://wiki.lsce.ipsl.fr/pmip3/doku.php/pmip3:design:21k:final`) and the PMIP2 protocol relied on the ICE-5G topography (Peltier, 2004). To account for the sea level difference between the LGM and PI, the protocol underlines that a higher salinity of 1 psu should be ensured during the initialization of the ocean. We expect that this would partly compensate for the temperature effect by reducing the CO_2 solubility.

For ocean biogeochemistry models specifically, Kageyama et al. (2017) also recommend that "the global amount of dissolved inorganic carbon (DIC), alkalinity, and nutrients should be initially adjusted to account for the change in ocean volume. This can be done by multiplying their initial value by the relative change in global ocean volume." The implicit modelling choice here is to ensure the mass conservation of these tracers. Running a LGM experiment from a PI restart, adjusting these variables will induce an increase of their concentration. We expect that this will impact the carbon storage capacity of the ocean. Indeed, increased nutrient concentrations can boost marine productivity and consequently affect the biological pump. In addition, an increase of alkalinity lowers atmospheric CO_2 concentrations by displacing the acid-base equilibriums of inorganic carbon in favour of CO_3^{2-} (Sigman et al., 2010). These adjustments are typically done by assuming a -3% decrease in total ocean volume (Brovkin et al., 2007), or a decrease close to this value (Morée et al., 2021; Bouttes et al., 2010). However, it should be noted that these adjustments are meant to account for the sea level change at a global scale, and do not reflect local processes such as corals or shelf erosion (Broecker, 1982). Studies suggest in particular that the reduced continental shelf area during glacial times may have led to an elevated whole ocean alkalinity via reduced carbonate deposition on shelves (Kerr et al., 2017; Rickaby et al., 2010). While changes in the alkalinity budget during glacial cycles remain debated, assuming a conserved inventory is a simple and frequent choice in models which do not include sediments.

2.2 The PMIP-carbon model outputs

Five General Circulation Models (GCMs: MIROC4m-COCO, CESM, MPI-ESM, IPSL-CM5A2, MIROC-ES2L) and four Earth System Models of intermediate complexity (EMICs: CLIMBER-2, iLOVECLIM, LOVECLIM, UVic) have performed carbon-cycle enabled LGM simulations submitted to the PMIP-carbon project. Most of them did not include additional glacial mechanisms (e.g. sediments, permafrost, brines, iron fertilization...) when running their LGM simulation, with the exception of MPI-ESM which includes an embedded sediment module (Ilyina et al., 2013), and MIROC4m-COCO, MIROC-ES2L, MPI-ESM and IPSL-CM5A2 in which dust-induced iron fluxes were changed at the LGM. These models and the characteristics of their LGM simulations are summed up in Table 1.

This table shows that PMIP-carbon model outputs result from differing modelling choices in terms of model resolution, boundary conditions, and CO_2 forcing (either prescribed at 190 ppm in both the radiative code and carbon cycle model, or prescribed in

Table 1. Characteristics of the LGM simulations of PMIP-carbon models. * indicates that the CO_2 concentration in both the radiative and the carbon cycle code is prescribed to 190 ppm, following the PMIP4 protocol which recommended a slight change of atmospheric CO_2 (compared to 185 ppm in PMIP3) to ensure consistency with the deglaciation protocol (Ivanovic et al., 2016).

Model name	Ocean resolution lat × lon (levels)	Atmospheric CO_2	Ice sheet reconstruction	Ocean boundary conditions	Adjustment of DIC, alkalinity, nutrients
MIROC4m	$\sim 1^\circ \times 1^\circ \times$ (43)	freely evolving	ICE-5G	unchanged	no
CLIMBER-2	$2.5^\circ \times 3$ basins (21)	freely evolving	ICE-5G	unchanged	yes (-3.3%)
CESM	$\sim 400 - 40$ km (60)	freely evolving	ICE-6G-C	changed	yes (-5.7%)
iLOVECLIM	$3^\circ \times 3^\circ$ (20)	freely evolving	GLAC-1D, ICE-6G-C	changed	yes (see Sect. 3.2)
MPI-ESM	$3^\circ \times 3^\circ$ (40)	prescribed	GLAC-1D	changed	yes (see SI)
IPSL-CM5A2	$2^\circ - 0.5^\circ$ (31)	prescribed*	PMIP3	changed	yes (-3%)
MIROC-ES2L	$1^\circ \times 1^\circ$ (63)	prescribed*	ICE-6G-C	changed	yes (-3%)
LOVECLIM	$3^\circ \times 3^\circ$ (20)	prescribed*	ICE-6G-C	unchanged	yes (-3.3%)
UVic	$3.6^\circ \times 1.8^\circ$ (19)	prescribed*	GLAC-1D, ICE-6G-C, PMIP3	changed	no

the radiative code but freely evolving in the carbon cycle part). In particular, the effects of a lower sea level are accounted for differently by the models. Ocean boundary conditions (i.e. bathymetry and coastlines) are not updated in three of the LGM experiments. Furthermore, the recommended initial adjustment of ocean biogeochemistry variables (Kageyama et al., 2017) to account for the change in ocean volume is not consistently applied. Indeed, when these three variables are adjusted, it is often according to a theoretical value of around -3%, rather than according to the relative volume change imposed in models. However, considering that the ocean boundary conditions stem from different ice sheet reconstructions and are interpolated on ocean grids of various resolution, the resulting ocean volumes and relative volume change may not always be equal to this theoretical value. These differing modelling choices give us the opportunity to evaluate their impact on the simulated carbon at the LGM.

2.3 Evaluating the ocean volume in PMIP models

We now focus on the total ocean volume, which conditions both the size of this carbon reservoir and the adjustment of biogeochemical variables. In models, topographic data are typically used to implement boundary conditions for the LGM (e.g. GLAC-1D, ICE-6G-C reconstructions) or PI (e.g. etopo1, Amante and Eakins (2009)). To quantify the impact of modelling choices related to the implementation of ocean boundary conditions on the ocean volume, we computed the ocean volumes of PMIP-carbon models for both the LGM and PI period. Then, we compared these values to the ocean volumes computed using topographic data (Fig. 1).

2.3.1 The ocean volume from topographic data

We computed the ocean volume from the ICE-6G-C and GLAC-1D topographies, both at 21 kyr and at 0 kyr (see dotted and dashed lines in Fig. 1). The ocean volume from the etopo1 topography was computed by Eakins and Sharman (2010): 1.335×10^{18} m^3 ($\pm$ 1%). These topographic data are of medium to high resolution: the ICE-6G-C topography is provided on a (1080, 2160) points grid and the GLAC-1D topography on a (360, 360) one. The etopo1 relief data have a 1 arc-minute resolution. Considering the high resolution of these data, we assume a relatively negligible error in the computed ocean volumes (with respect to reality). We use these reference values to quantify the differences (Δ) linked with the interpolation on a coarser grid and/or with modelling choices made during the implementation of boundary conditions (Table 2).

We observe that the ocean volumes associated with the ICE-6G-C and GLAC-1D topographies at 0 kyr are similar to the etopo1 ocean volume (see dotted lines on Fig.

1). However, there is a difference of around 1×10^{16} m^3 between the volumes computed at the LGM (see dashed lines on Fig. 1): we found 1.299×10^{18} m^3 (GLAC-1D), 1.292×10^{18} m^3 (ICE-6G-C) and 1.288×10^{18} m^3 (ICE-5G). This difference stems from the uncertainties in ice sheet reconstructions. As the Laurentide ice sheet is higher in the ICE-6G-C reconstruction than in the GLAC-1D one (Kageyama et al., 2017), the ocean volume calculated from ICE-6G-C is consistent with a lower sea level. From these reconstructions, we computed a LGM−PI volume difference of around -4.30 $\times 10^{16}$ m^3 (ICE-6G-C−etopo1). We note that running LGM simulations from a PI restart entails in theory a relative volume change of -2.72% (GLAC-1D), -3.22% (ICE-6G-C), or -3.48% (ICE-5G) when this volume change is computed relative to the PI ocean volume from etopo1 topography ; or -2.88% (GLAC-1D) and -3.19% (ICE-6G-C) when considering the ICE-6G-C and GLAC-1D topographies at 0 kyr. These values are close to the -3% change enforced in the initial adjustment of biogeochemical variables in some PMIP-carbon models (Table 1).

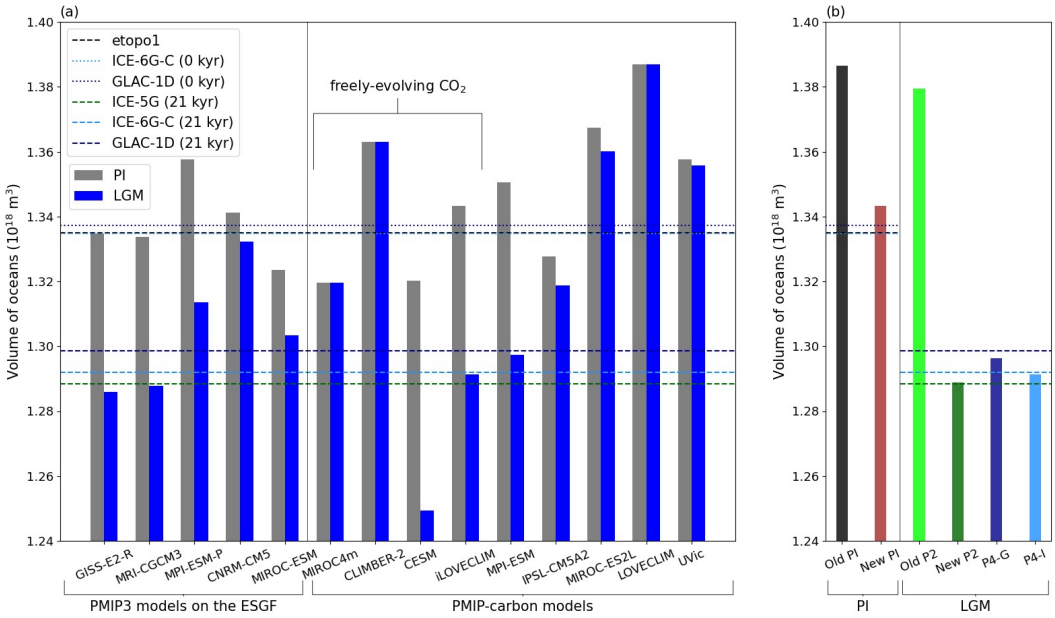

Figure 1. Ocean volume in (a) PMIP models and (b) iLOVECLIM simulations. The iLOVECLIM reference simulations in (a) are 'New PI' and 'P4-I'. The dashed and dotted lines represent the ocean volume computed from high resolution topographic files (etopo1, ICE-5G, GLAC-1D, and ICE-6G-C).

2.3.2 The ocean volume implemented in PMIP models

We used the fixed fields for each PMIP-carbon model to compute the total integrated ocean volume. To provide more elements of comparison, we also computed the ocean volumes of additional PMIP3 models. We chose the GISS-E2-R, MRI-CGCM3, MPI-ESM-P, CNRM-CM5 and MIROC-ESM models since both their LGM and PI fixed fields were available for download.

The PMIP models show a large range of ocean volumes for their PI and LGM states, and a range of LGM−PI volume changes (Fig 1a and Table 2). The difference (Δ) with the computed volume based on high resolution topographic data (etopo1, ICE-6G-C) is significant for the majority of models: this difference amounts to less than 1% for only 6 models (out of 14) at the PI and for only 5 models at the LGM. The PMIP models

Table 2. Quantification in PMIP models of PI and LGM ocean volumes, as well as the volume changes between the LGM simulation and its PI restart (LGM−PI, that is to say a PI-to-LGM change). Their differences (Δ) with respect to the ocean volume computed from PI (etopo1) and/or from LGM topographic data (ICE-6G-C, 21 kyr) are shown, indicating when an overestimated PI volume (Δ PI > 0%), LGM volume (Δ LGM > 0%), or volume change (Δ LGM−PI > 0%) seems to be observed. The relative volume change in models can also be compared to the one computed from topographic data: -2.88% (GLAC-1D) or -3.19% (ICE-6G-C).

Project	Model name	PI (10^{18} m^3)	LGM (10^{18} m^3)	Δ PI (%)	Δ LGM (%)	LGM−PI (10^{16} m^3)	Δ LGM−PI (%)	Relative change (%)
PMIP3	GISS-E2-R	1.335	1.286	-0.02	-0.48	-4.89	+13.73	-3.66
	MRI-CGCM3	1.334	1.288	-0.09	-0.33	-4.59	+6.92	-3.44
	MPI-ESM-P	1.358	1.313	+1.70	+1.66	-4.42	+2.93	-3.26
	CNRM-CM5	1.341	1.332	+0.47	+3.11	-0.91	-78.91	-0.68
	MIROC-ESM	1.323	1.303	-0.86	+0.88	-2.01	-53.32	-1.52
PMIP-carbon	MIROC4m	1.320	1.320	-1.16	+2.13	0	-100	0
	CLIMBER-2	1.363	1.363	+2.10	+5.49	0	-100	0
	CESM	1.320	1.249	-1.12	-3.25	-7.10	+65.34	-5.38
	iLOVECLIM	1.343	1.291	+0.62	-0.05	-5.19	+20.85	-3.87
	MPI-ESM	1.351	1.297	+1.17	+0.40	-5.33	+24.08	-3.95
	IPSL-CM5A2	1.328	1.319	-0.54	+2.07	-0.90	-79.05	-0.68
	MIROC-ES2L	1.367	1.360	+2.42	+5.26	-0.73	-83.09	-0.53
	LOVECLIM	1.387	1.387	+3.90	+7.35	0	-100	0
	UVic	1.358	1.356	+1.70	+4.93	-0.20	-95.33	-0.15

with an ocean volume close to the high resolution topographic data at both the PI and the LGM are MRI-CGCM3, GISS-E2-R, iLOVECLIM and MPI-ESM (PMIP4). MPI-ESM-P (PMIP3) shows a slight overestimation (+1.7%) for both its PI and LGM volume but its relative volume change remains realistic (-3.26%). However, the LGM−PI difference is often largely underestimated (CNRM-CM5, MIROC-ESM, IPSL-CM5A2, MIROC-ES2L, UVic) or not implemented at all (MIROC4m-COCO, CLIMBER-2, LOVECLIM). As a result, these 8 models significantly underestimate the relative volume change (-0% to -1.52%). Finally, CESM underestimates both the PI and the LGM volumes while being the only model largely overestimating the relative volume change (-5.38%). Although a majority of models substantially underestimate the relative volume change, the LGM−PI difference in ocean surface area is less frequently underestimated (Fig. S1). This suggests that the coastlines associated with the low sea level of the LGM may have been set more carefully than the bathymetry.

We note that EMICs (CLIMBER-2, LOVECLIM, UVic) tend to substantially overestimate the PI ocean volume with respect to etopo1 data. They also show little to no change in ocean boundary conditions at the LGM (Fig. 1a and Table 2). This is not the case of the iLOVECLIM model, which will be further detailed in Sect. 3.1 and in Fig. 1b. Conversely, most GCMs also show discrepancies with the ocean volumes of topographic data at both the PI and LGM (CESM, MPI and MIROC models) or mainly at the LGM (CNRM-CM5, IPSL-CM5A2). There is no obvious correlation between model spatial resolution and ocean volume accuracy.

Since PMIP-carbon models simulate various change of ocean volume, we expect different responses of the carbon cycle to these differing ocean boundary conditions. Indeed, the simulated ocean carbon concentrations, which depend both on mass and volume, may be merely affected by a reservoir size effect. In particular, models with a large ocean volume at the LGM may overestimate carbon storage in the ocean. Moreover, the adjustment of biogeochemical variables done in some LGM simulations (e.g. according to a theoretical −3% change) is not necessarily consistent with the ocean volume change enforced in the models, which leads to a failed mass conservation of these tracers. It is difficult to assess the consequences of these bathymetry related modelling choices on the simulated carbon at the LGM by relying only on PMIP-carbon model outputs: these models also have differing carbon cycle modules, simulate different climate backgrounds, and do not all simulate a freely evolving CO_2 in the carbon cycle (Table 1). Therefore, we

sought to evaluate the impact of these choices using additional sensitivity tests run with the iLOVECLIM model (see Appendix).

3 Evaluating the impact of bathymetry related modelling choices on the simulated carbon at the LGM

3.1 Ocean boundary conditions in the iLOVECLIM model and resulting ocean volumes

As shown in Table 1, the iLOVECLIM LGM simulations were run with with a freely evolving CO_2 in the carbon cycle and following the PMIP4 experimental design (Kageyama et al., 2017). We used either the GLAC-1D or the ICE-6G-C ice sheet reconstruction to implement the boundary conditions (including the bathymetry and coastlines), thanks to the new semi-automated bathymetry generation method described in Lhardy et al. (2021). We also implemented new ocean boundary conditions for the PI, using a modern high resolution topography file (etopo1) to replace the old bathymetry (adapted from etopo5, 1986). As this change of ocean boundary conditions has an impact on the ocean volume and therefore on the size of this carbon reservoir (Fig. 1b), we retuned the total carbon content at the PI in order to get an equilibrated atmospheric CO_2 concentration of around 280 ppm. This content is now 632 GtC lower (41,016 GtC compared to 41,647 GtC previously). To ensure equilibrium, we then ran 5000 years of LGM carbon simulation using this PI restart called 'New PI'. The two standard LGM simulations (run following the PMIP4 protocol, using either the GLAC-1D or ICE-6G-C topography) are called 'P4-G' and 'P4-I' respectively. To observe the effect of the semi-automated bathymetry generation method on the ocean volume, in our study we use the fixed fields of simulations run with the former PI and LGM bathymetries (respectively 'Old PI' and 'Old P2'). As the latter was manually generated in the framework of the PMIP2 exercise, we also regenerated with this method the bathymetry and coastlines associated with the ICE-5G topography recommended in the PMIP2 protocol. The resulting 'New P2' simulation is therefore more comparable to 'Old P2' than the 'P4-G' and 'P4-I' simulations. All these simulations are also described in Table 3.

Table 3. iLOVECLIM simulations with differing ocean boundary conditions (BCs, i.e. coastlines and bathymetry), hence the differing ocean volumes shown in Fig. 1b.

Simulation name	Old PI	New PI	Old P2	New P2	P4-G	P4-I
PMIP protocol	-	-	PMIP2	PMIP2	PMIP4	PMIP4
Ocean BCs from	etopo5 (1986)	etopo1 (2009)	ICE-5G	ICE-5G	GLAC-1D	ICE-6G-C
Generation method	manual	semi-automated	manual	semi-automated	semi-automated	semi-automated

Figure 1b shows that with the implementation of manually tuned bathymetries, the former version of iLOVECLIM was run with overestimated ocean volumes at the PI (+3.86% for 'Old PI') and especially at the LGM (+7.06% for 'Old P2'). Most of the overestimation of the 'Old P2' ocean volume is caused by differences in the deepest (deeper than 4 km) grid cells (Fig. S2), rather than the slight overestimation of the ocean surface area (Fig. S1b). As a result, iLOVECLIM used to simulate only 15% of the LGM−PI volume change (Table S1). However, we now have much more realistic ocean volume values in the current version of iLOVECLIM, both at the PI ('New PI') and at the three new LGM simulations ('New P2', 'P4-G' and 'P4-I'). Indeed, these values are all fairly close to their references (etopo1, ICE-5G, GLAC-1D and ICE-6G-C respectively), though there is still a small overestimation of the PI ocean volume. Despite the interpolation of the bathymetry on a relatively coarse ocean grid, it is interesting to note that the differences (Δ) with respect to topographic data are now of the same order of magnitude as other GCMs of higher resolution (Table 1), and smaller than most models. Since this improvement can be attributed to the bathymetry generation method which notably leads

to a reduced number of deep and voluminous grid cells in iLOVECLIM LGM runs (Fig. S2), we speculate that the effect of the sea level drop in abyssal plain areas is regularly overlooked in models.

3.2 Modelling choices related to the boundary conditions change and set of LGM simulations with iLOVECLIM

We made several modifications to the code of iLOVECLIM to allow for a change of ocean boundary conditions in an automated way. These developments allow us to run carbon simulations with the iLOVECLIM model under any given change of ocean boundary conditions (PI, GLAC-1D, ICE-6G-C or otherwise). First, we ensured a systematic conservation of salt. Indeed, the boundary conditions changes associated with a lower glacial sea level cause a loss of the salt contained in some grid cells such as the ones corresponding to the continental shelves. In LGM runs, 1 psu is usually added to the pre-industrial salinity to compensate for this loss (Kageyama et al., 2017). We computed the total salt content before and after initialization and the lost salt was added uniformly over the whole deep ocean (> 1 km). In iLOVECLIM, this automated modification is equivalent to an addition of 0.96 psu (GLAC-1D boundary conditions) or 1.11 psu (ICE-6G-C) to the pre-industrial salinity. Secondly, we coded an automated adjustment of ocean biogeochemistry variables. We chose to conserve the total alkalinity, nitrate and phosphate concentrations, and DIC, instead of multiplying their initial values by a relative volume change. This choice allows us to take into account not only the global sea level change, but also the distribution patterns of the tracers which would have been lost during the change of boundary conditions. Finally, the change of bathymetry and coastlines from PI to LGM conditions can also cause a loss in the ocean organic carbon pools (i.e. phytoplankton, zooplankton, dissolved organic carbon, particulate organic carbon and calcium carbonate). To account for it, we ensured an automated conservation of the total model carbon content. We computed the total carbon content before and after initialization and the carbon from organic pools which would have been lost was put into the atmosphere, which then re-equilibrated with the ocean during the run.

Table 4. Bathymetry related modelling choices of the LGM simulations with iLOVECLIM. Ocean boundary conditions (BCs, i.e. coastlines, bathymetry, and the resulting ocean volume) are specified by the letters G (GLAC-1D), I (ICE-6G-C) or PI (etopo1). Crosses indicate that the automated conservation of salt and carbon and adjustment of biogeochemical variables are done according to the relative change of volume (here relative to the PI restart). Hyphens indicate that these adjustments are inactive due to the absence of ocean boundary conditions change. 'no' indicates in which simulation these adjustments are deliberately switched off and 'yes' when they are done according to a theoretical value (-3.22%, the relative change of volume ~~between~~from etopo1 to ICE-6G-C).

Simulation name	P4-G	P4-I	salt-	C-	DIC-/C-	nut-	alk-	PIbathy	PIbathy,alk+
Ocean BCs	G	I	I	I	I	I	I	PI	PI
Salt conservation	×	×	no	×	×	×	×	–	–
Carbon conservation	×	×	×	no	no	×	×	–	–
DIC adjustment	×	×	×	×	no	×	×	–	–
Nutrients adjustment	×	×	×	×	×	no	×	–	–
Alkalinity adjustment	×	×	×	×	×	×	no	–	yes

We aim at quantifying the impact of modelling choices which relate to the change of ocean boundary conditions on the simulated carbon, that is:

- adjustments of alkalinity, nutrients, DIC
- automated conservation of the total salt content
- automated conservation of the total carbon content, as described above

To do this, we ran sensitivity tests using the ICE-6G-C boundary conditions (like 'P4-I') but without one or two of these choices: these simulations are called 'alk-', 'nut-', 'DIC-/C-', 'C-' and 'salt-'. To be clear, 'alk', 'nut' and 'DIC' refer to the adjustments of alkalinity, nutrients and DIC, while 'C' refers to the total carbon content conservation and 'salt' to the total salt content conservation. We ran 'DIC-/C-' both without the DIC ajustment and without the total carbon content conservation to be able to see the impact of the DIC adjustment. As a matter of fact, a 'DIC-' simulation (not shown here) results in the same carbon distribution in reservoirs as the reference 'P4-I', albeit after a longer equilibration time. Indeed, the total carbon content conservation − ensured by transferring the lost carbon to the atmosphere − makes up for the missing DIC adjustment, though the ocean and atmosphere need more time to re-equilibrate.

As the ocean boundary conditions are not always implemented in LGM simulations of PMIP-carbon models, we also ran a LGM simulation with the PI coastlines and bathymetry (called 'PIbathy'). As a consequence, there was no change of ocean volume nor any adjustment of biogeochemical variables during the initialization of this simulation. Finally, this ensemble of simulations is completed by 'PIbathy, alk+'. In this LGM simulation with the PI ocean boundary conditions, we increased the initial alkalinity according to a theoretical relative change of volume, since this is a modelling choice of some PMIP-carbon models. All simulations and the modelling choices related to the change of boundary conditions are summed up in Table 4.

3.3 Simulated carbon at the LGM

To assess the impact on the simulated carbon of these modelling choices which relates to the change of ocean boundary conditions, we computed the carbon content of each carbon reservoir (atmosphere, ocean, terrestrial biosphere) in PMIP-carbon models and iLOVECLIM sensitivity tests. Typically for the ocean, the concentration in each carbon pool (e.g. DIC, dissolved organic carbon, particulate carbon, phytoplankton...) was summed, integrated on the ocean grid (weighted by the grid cell volume), and converted into GtC. The equilibrated atmospheric CO_2 concentrations of PMIP-carbon models with freely evolving CO_2 in the carbon cycle are presented in Fig. 2a. The interested reader will find the carbon content of all reservoirs and models in Fig. S3.

Among the PMIP-carbon models, about half have thus far run with a freely evolving CO_2 for the carbon cycle (MIROC4m-COCO, CLIMBER-2, CESM and iLOVECLIM). Furthermore, among this subset, only CESM and iLOVECLIM are fully comparable in terms of carbon outputs, as they both have run with LGM ocean boundary conditions and include a vegetation model. We observe that these two models both typically simulate high CO_2 concentrations at the LGM (331 ppm and 315 ppm respectively, see Fig. 2a). These values are very far from the CO_2 levels inferred from data (∼190 ppm, Bereiter et al. (2015); Ivanovic et al. (2016)) as they are even higher than the PI levels (280 ppm).

3.3.1 In iLOVECLIM

Table 5. Quantification in iLOVECLIM simulations of the carbon content in reservoirs (GtC) and differences (GtC) with respect to 'P4-I'

Simulation name	New PI	P4-G	P4-I	salt-	C-	DIC-/C-	nut-	alk-	PIbathy	PIbathy,alk+
Atmosphere (GtC)	599	674	671	653	643	467	681	924	650	478
Ocean (GtC)	38,480	38,7628	38,753	38,767	38,627	37,599	38,742	38,499	39,020	39,191
Vegetation (GtC)	1,937	1,615	1,593	1,596	1,593	1,593	1,593	1,593	1,347	1,347
Atmosphere difference	-72	+3	0	-18	-28	-204	+10	+254	-21	-192
Ocean difference	-272	-25	0	+14	-126	-1153	-10	-253	+267	+439
Vegetation difference	+344	+22	0	+3	0	0	0	0	-246	-246

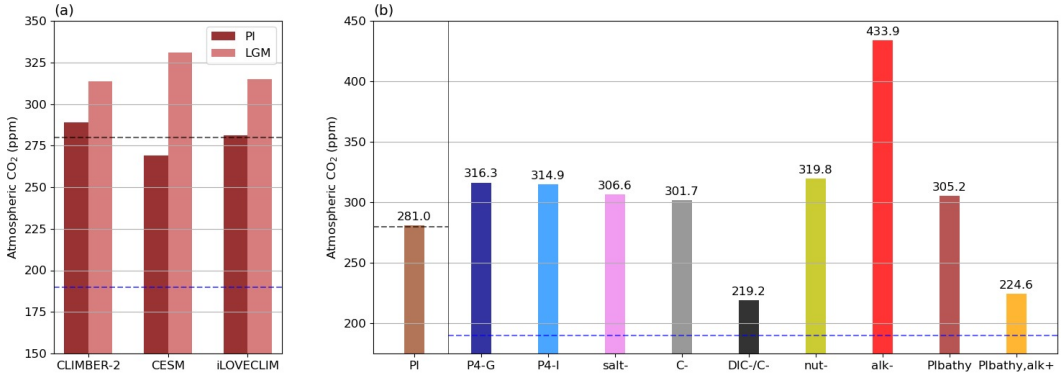

Figure 2. Atmospheric CO_2 (ppm) in (a) PMIP-carbon models with a freely evolving CO_2 in the carbon cycle (excluding the ocean-only MIROC4m-COCO) and (b) iLOVECLIM simulations. The iLOVECLIM reference simulations in (a) are 'New PI' and 'P4-I'. The grey and blue dashed lines represents the atmospheric CO_2 concentrations at the PI (280 ppm) and LGM (190 ppm, Bereiter et al. (2015)).

Looking at the carbon distribution simulated in the different reservoirs by the iLOVECLIM model (Table 5), we observe that although the ocean volume is smaller, the ocean is effectively trapping more carbon at the LGM (+272 GtC for 'P4-I' compared to 'New PI'). However, the terrestrial biosphere sink is also less efficient due to lower temperatures and the presence of large ice sheets (-344 GtC). Overall, it results in higher atmospheric concentrations as the ocean sink is not enhanced enough to compensate for the smaller terrestrial biosphere sink. The carbon outputs from the two standard LGM simulations ('P4-G' and 'P4-I') suggest that the ice sheet reconstruction (GLAC-1D or ICE-6G-C) chosen to implement the boundary conditions has a small impact on the simulated carbon (as well as the ocean volume, see Fig. 1b and Table S1).

Using the iLOVECLIM sensitivity tests, we quantify the carbon content variations associated with the modelling choices made to accomodate the change of ocean boundary conditions. If the total salt content conservation is not ensured ('salt-'), we get slightly lower CO_2 concentrations (8 ppm lower), as the CO_2 solubility is greater when the salinity is lower. The total carbon content conservation apparently has a relatively small effect on the CO_2 (13 ppm lower), but is actually essential when the DIC adjustment is not done either ('DIC-/C-'): in this case, 1,357 GtC are lost, and the CO_2 concentration is much closer to the LGM data value but for the wrong reason, that is a loss of total carbon from the system. Only 154 GtC are lost in the 'C-' simulation, which amount to the lost organic carbon. Indeed, the DIC adjustment compensates for most of the lost carbon as the DIC is the largest carbon pool in the ocean. As for the other two recommended adjustments, the nutrient adjustment has a relatively small effect through a marine productivity boost (+5 ppm without it, see 'nut-') whereas the alkalinity adjustment is much more critical. Indeed, the simulation without it ('alk-') has a CO_2 reaching as high as 434 ppm: an increased alkalinity reduces the atmospheric CO_2 concentration (by 254 GtC). Given the large effect of this adjustment, the method used to implement it is crucial.

In addition, we quantify the carbon content simulated at the LGM with no change of ocean boundary conditions in iLOVECLIM. We see from the 'PIbathy' simulation that a larger ocean volume can significantly increase the ocean carbon content at the LGM (+267 GtC, close to a doubling of the LGM−PI difference), but in this instance at the expense of the terrestrial carbon (-246 GtC). This difference in terrestrial carbon content can be explained by the second ocean boundary condition, as the PI coastlines yield less available land surfaces to grow vegetation. While this compensation of errors causes

a relatively small change of atmospheric CO_2 concentration, we argue here that not changing the bathymetry while performing LGM experiments significantly affects the carbon distribution since it can potentially trap twice as much carbon in the ocean. Furthermore, if this absence of ocean boundary conditions change is combined with the adjustment of alkalinity (considering the theoretical relative volume change between etopo1 and ICE-6G-C, see 'PIbathy,alk+'), the carbon storage of the ocean is increased even more. This time, the drop of atmospheric CO_2 concentration is much more significant as there is no addidional compensating effect of the terrestrial biosphere.

3.3.2 In PMIP-carbon models

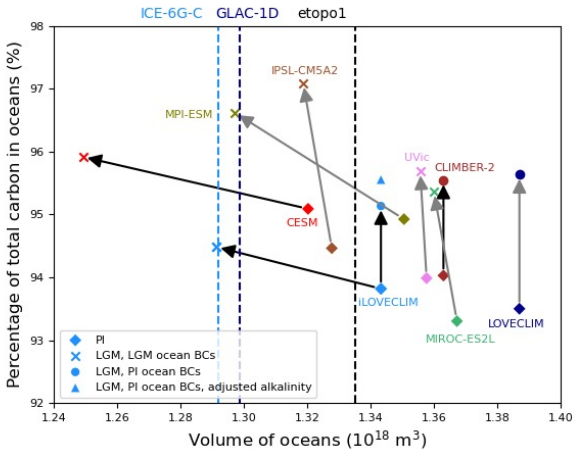

Figure 3. Ocean carbon versus ocean volume plot for a subset of PMIP-carbon models (excluding the ocean-only MIROC4m-COCO) and iLOVECLIM simulations ('P4-I', 'PIbathy' and 'PIbathy,alk+'). The dashed lines represent the ocean volume computed from high resolution topographic files (etopo1, GLAC-1D, ICE-6G-C). The PI to LGM changes are traced by the grey (prescribed CO_2) and black (freely evolving CO_2) arrows. BCs stands for boundary conditions.

Finally, since the ocean is thought to have played a major role in explaining the pCO_2 drawdown at the LGM, we now examine the ocean carbon content simulated by PMIP-carbon models in light of our findings on ocean volume. We know that PMIP-carbon models simulate various total carbon content (Fig. S3b). To be able to compare their carbon content in the ocean, we therefore plotted in Fig. 3 the percentage of carbon in the ocean at the PI and LGM, against the ocean volume. Figure 3 clearly shows four distinct model behaviours. CLIMBER-2 and LOVECLIM, which have run with no change of ocean boundary conditions, show a significantly larger proportion of carbon in the oceans under LGM conditions (+1.5% and +2.1% respectively). IPSL-CM5A2, MIROC-ES2L and UVic have run with a limited change of ocean volume, and they also simulate a large increase of carbon storage in the oceans between their PI and LGM states (+2.6%, +2.1% and 1.7% respectively). In contrast, the ocean carbon content of iLOVECLIM and CESM increases at the LGM, but this variation (+0.7% and +0.8%) is relatively smaller than in other models with no large change of ocean boundary conditions. The exception is MPI-ESM, which displays both a large change of ocean volume and carbon storage (+1.7%). It is however not fully comparable to iLOVECLIM and CESM models as it also ran with a prescribed CO_2 in the carbon cycle. Finally, we underline that the two iLOVECLIM simulations with no change of ocean volume show a larger increase of carbon storage in the oceans (+1.3% and +1.7% for 'PIbathy' and 'PIbathy,alk+' respectively). Therefore, it is likely that other models would also simulate lower carbon sequestration in the

oceans and high atmospheric CO_2 concentration values (much larger than 190 ppm, if freely-evolving) if they had a lower ocean volume at the LGM.

4 Discussion and conclusion

In this study, we use preliminary results of the PMIP-carbon project and sensitivity tests run with the iLOVECLIM model at the LGM to quantify the consequences of bathymetry related modelling choices on the simulated carbon at the global scale. We consider the effects of the ocean volume change and of the resulting biogeochemical variables adjustments recommended in Kageyama et al. (2017).

We show that the implementation of ocean boundary conditions in PMIP models rarely results in accurate ocean volumes. We suggest that this may not be primarily related to the model resolution, since we get a much more realistic ocean volume in iLOVECLIM after developing a new method to generate the bathymetry despite the relatively coarse resolution of its ocean model. In fact, the ocean boundary conditions (i.e. bathymetry, coastlines) associated with the low sea level of the LGM are not systematically generated in models. When they are, modelling groups often mostly concentrate on setting the coastlines ("land-sea mask") and the bathymetry of shallow grid cells in order to simulate a reasonable ocean circulation. However, the ocean volume is mostly affected by the bathymetry of deep grid cells in models with irregular vertical levels. Setting the bathymetry of these deep grid cells to account for a sea level of -134 m (Lambeck et al., 2014) at the LGM, even if the vertical resolution exceeds such a value, will move up the ocean floor here and there depending on the outcome of vertical interpolation. As a result, the overall volume of deep levels should be closer to reality. It is therefore important to account for the -134 m sea level change before the vertical interpolation done to generate the bathymetry in order to implement a realistic volume change between PI and LGM.

While these modelling choices may have little consequences on the climate variables usually examined in PMIP intercomparison papers, we argue that their effects on the simulated carbon cannot be overlooked, considering the role of the deep ocean on carbon storage (Skinner, 2009). In the iLOVECLIM model, the carbon distribution in reservoirs is significantly affected when the low sea level is not taken into account. Indeed, in the absence of a change of ocean boundary conditions in LGM runs, the carbon sequestration in the ocean is increased twofold due to the larger size of this reservoir. In contrast, more carbon is lost in the terrestrial biosphere as the coastlines of the PI do not allow for emerged continental shelves to grow vegetation. While different model biases may limit carbon sequestration in the ocean (e.g. underestimated stratification, sea ice, efficiency of the biological pump), an overestimated ocean volume at the LGM has an opposite effect. It is therefore even more challenging for models with a realistic ocean volume at the LGM to simulate the pCO_2 drawdown.

Kageyama et al. (2017) recommend an adjustment of DIC, nutrients and alkalinity to account for the change of ocean volume between the PI and the LGM. We quantify the effects of each on the simulated carbon at the LGM in the iLOVECLIM model. The DIC adjustment shortens the equilibration time but is not essential as long as carbon conservation is otherwise ensured. We observe a limited effect of the nutrients adjustment but adjusting the alkalinity yields a large increase of carbon sequestration in the ocean ($\sim$ 250 GtC). As a result, this last adjustment should be cautiously made. Multiplying the initial alkalinity by a theoretical value of around 3% which is potentially far from the implemented relative change of volume can significantly decrease the atmospheric CO_2 concentration.

The quantified effects of these modelling choices in iLOVECLIM depend on the carbon cycle module and on the simulated climate (e.g. surface temperatures, deep ocean circulation, sea ice). In that respect, quantifications using other models would be useful to assess the robustness of these results, which can be affected by model biases. Further studies using coupled carbon-climate models including sediments may be especially desirable to be able to compute the alkalinity budget from riverine inputs and $CaCO_3$

burial (Sigman et al., 2010), as accounting for this mechanism may significantly increase the simulated pCO_2 drawdown (Brovkin et al., 2007, 2012; Kobayashi & Oka, 2018). Still, these results give us a sense of the magnitude of each effect. We stress here that the ocean volume and the alkalinity adjustment should be both carefully considered in coupled carbon-climate simulations at the LGM as there is a risk of simulating a low CO_2 for the wrong reasons.

At present, PMIP-carbon models with a freely evolving CO_2 are all simulating an increased carbon sequestration into the ocean at the LGM, but also high atmospheric concentrations (> 300 ppm). Overall, the enhanced carbon sink of the ocean is therefore not compensating for the loss of carbon in the terrestrial biosphere due to the lower temperatures and extensive ice sheets. Causes for the glacial CO_2 drawdown can be sought inside (e.g. physical and biogeochemical biases, Morée et al. (2021)) or outside (e.g. iron, terrestrial vegetation, sediments, permafrost) of the modelled ocean. However, investigating the processes behind the pCO_2 drawdown at the LGM and their limitations in model representation remains a challenge insofar as model outputs are hardly comparable. Our findings emphasize the need for documenting the ocean volume in models and defining a stricter protocol for PMIP-carbon models with the view of improving coupled climate-carbon simulations intercomparison potential. One practical recommendation in future PMIP protocols could be to enforce an alkalinity adjustment based on the actual (rather than theoretical) change of ocean volume implemented in biogeochemistry models at the LGM. Explicit guidelines concerning the change of ocean volume and related modelling choices may also be relevant for other target periods of paleoclimate modelling.

Appendix A Description of the iLOVECLIM model under the PMIP experimental design

The iLOVECLIM model (Goosse et al., 2010) is an EMIC. Its standard version includes an atmospheric component (ECBilt), a simple land vegetation module (VECODE) and an ocean general circulation model named CLIO, of relatively coarse resolution ($3° \times 3°$ and 20 irregular vertical levels). In addition, a carbon cycle model is fully coupled to these components. Originated from a NPZD ecosystem model (Six & Maier-Reimer, 1996), it was further developed in the CLIMBER-2 model (Brovkin, Bendtsen, et al., 2002; Brovkin, Hofmann, et al., 2002; Brovkin et al., 2007) before it was also implemented in iLOVECLIM (Bouttes et al., 2015).

The iLOVECLIM model is typically used to simulate past climates such as the LGM, and contributed to previous PMIP exercises (Roche et al., 2012; Otto-Bliesner et al., 2007) under its PMIP2 version (Roche et al., 2007), as well as to the current PMIP4 exercise (Kageyama et al., 2021). The LGM simulations run with iLOVECLIM follow the standardized experimental design described in the PMIP4 protocol (Kageyama et al., 2017). In order to assess the impact of the ice sheet reconstruction choice, we implemented the boundary conditions associated with the two most recent reconstructions (GLAC-1D and ICE-6G-C, both recommended in Ivanovic et al. (2016)) in the iLOVECLIM model, using a new semi-automated bathymetry generation method described in Lhardy et al. (2021). The change of bathymetry and coastlines was automated for the most part, with a few unavoidable manual changes in straits and key passages. We also implemented new ocean boundary conditions for the PI, using a modern high resolution topography file (etopo1, Amante and Eakins (2009)) to replace the old bathymetry (adapted from etopo5, 1986).

Acknowledgments

The model outputs of PMIP-carbon models and iLOVECLIM simulations are available for download online (doi: 10.5281/zenodo.5464162). The fixed fields of GISS-E2-R, MRI-CGCM3, MPI-ESM-P, CNRM-CM5 and MIROC-ESM models can also be found at `https://esgf-node.llnl.gov/projects/cmip5/`. Descriptions of the PMIP-carbon

models can be found in Kobayashi and Oka (2018) (MIROC4m-COCO), Petoukhov et al. (2000) and Ganopolski et al. (2001) (CLIMBER), Bouttes et al. (2015) and Lhardy et al. (2021) (iLOVECLIM), Liu et al. (2021), Mauritsen et al. (2019) and references therein (MPI-ESM), Ohgaito et al. (2021) and Hajima et al. (2020) (MIROC-ES2L).

FL, NB and DMR designed the research. NB coordinated the PMIP-carbon project and obtained funding. Participating modelling groups all performed a PI and a LGM simulation, provided their model outputs and the relevant metadata and computed the equilibrated carbon content in reservoirs. These modelling groups included AA-O, HK and AO (MIROC4m-COCO) ; KC (CLIMBER-2) ; MJ, RN, GV and ZC (CESM) ; BL and TI (MPI-ESM); MK (IPSL-CM5A2) ; AY (MIROC-ES2L) ; LM (LOVECLIM) ; JM and AS (UVic). FL, DMR and NB generated new boundary conditions in the iLOVECLIM model. NB and DMR developed the automated adjustments to allow for a change of ocean boundary conditions. FL ran the iLOVECLIM simulations and analyzed both the iLOVECLIM and the PMIP-carbon outputs under supervision of NB and DMR. FL wrote the manuscript with the inputs from all co-authors.

This study was supported by the French National program LEFE (*Les Enveloppes Fluides et l'Environnement*). FL is supported by the *Université Versailles Saint-Quentin-en-Yvelines* (UVSQ). NB and DMR are supported by the *Centre national de la recherche scientifique* (CNRS). In addition, DMR is supported by the Vrije Universiteit Amsterdam. BL and TI are supported by the German Federal Ministry of Education and Research (PalMod initiative, FKZ: 420 grant no. 01LP1919B). LM acknowledges funding from the Australian Research Council grant FT180100606. AY acknowledges funding from the Integrated Research Program for Advancing Climate Models (TOUGOU) Grant Number JPMXD0717935715 from the Ministry of Education, Culture, Sports, Science and Technology (MEXT), Japan. We acknowledge the use of the LSCE storage and computing facilities. We thank Théo Mandonnet for his preliminary work on the PMIP-carbon project. Last but not least, we thank the two anonymous reviewers for their help with this manuscript.

The authors declare that they have no conflict of interest.

References

Abe-Ouchi, A., Saito, F., Kageyama, M., Braconnot, P., Harrison, S. P., Lambeck, K., ... Takahashi, K. (2015). Ice-sheet configuration in the CMIP5/PMIP3 Last Glacial Maximum experiments. *Geosci. Model Dev.*, *8*, 3621–3637. doi: 10.5194/gmd-8-3621-2015

Aldama-Campino, A., Fransner, F., Ödalen, M., Groeskamp, S., Yool, A., Döös, K., & Nycander, J. (2020). Meridional Ocean Carbon Transport. *Global Biogeochem. Cy.*. doi: 10.1029/2019GB006336

Amante, C., & Eakins, B. W. (2009). ETOPO1 1 Arc-Minute Global Relief Model: Procedures, Data Sources and Analysis. NOAA Technical Memorandum NESDIS NGDC-24. National Geophysical Data Center, NOAA. `https://www.ngdc.noaa.gov/mgg/global/global.html`. doi: 10.7289/V5C8276M

Anderson, R. F., Sachs, J. P., Fleisher, M. Q., Allen, K. A., Yu, J., Koutavas, A., & Jaccard, S. L. (2019). Deep-Sea Oxygen Depletion and Ocean Carbon Sequestration During the Last Ice Age. *Global Biogeochem. Cy.*, *33*, 301–317. doi: 10.1029/2018GB006049

Argus, D. F., Peltier, W. R., Drummond, R., & Moore, A. W. (2014). The Antarctica component of postglacial rebound model ICE-6G-C (VM5a) based on GPS positioning, exposure age dating of ice thicknesses, and relative sea level histories. *Geophysical Journal International*, *198*, 537–563. doi: 10.1093/gji/ggu140

Bereiter, B., Eggleston, S., Schmitt, J., Nehrbass-Ahles, C., Stocker, T. F., Fischer, H., ... Chappellaz, J. (2015). Revision of the EPICA Dome C CO_2 record from 800 to 600 kyr before present. *Geophys. Res. Lett.*, *42*, 542–549. doi:

10.1002/2014GL061957

Bopp, L., Kohfeld, K. E., & Le Quéré, C. (2003). Dust impact on marine biota and atmospheric CO_2 during glacial periods. *Paleoceanography*, *18*(2). doi: 10.1029/2002PA000810

Bouttes, N., Paillard, D., & Roche, D. M. (2010). Impact of brine-induced stratification on the glacial carbon cycle. *Clim. Past*, *6*(5), 575–589. doi: 10.5194/cp-6-575-2010

Bouttes, N., Roche, D. M., Mariotti, V., & Bopp, L. (2015). Including an ocean carbon cycle model into iLOVECLIM (v1.0). *Geoscientific Model Development*, *8*, 1563–1576. doi: 10.5194/gmd-8-1563-2015

Broecker, W. S. (1982). Ocean chemistry during glacial time. *Geochimica et Cosmochimica Acta*, *46*, 1689–1705.

Brovkin, V., Bendtsen, J., Claussen, M., Ganopolski, A., Kubatzki, C., Petoukhov, V., & Andreev, A. (2002). Carbon cycle, vegetation, and climate dynamics in the Holocene: Experiments with the CLIMBER-2 model. *Global Biogeochem. Cy.*, *16*. doi: 10.1029/2001GB001662

Brovkin, V., Ganopolski, A., Archer, D., & Munhoven, G. (2012). Glacial CO_2 cycle as a succession of key physical and biogeochemical processes. *Clim. Past*, *8*, 251–264. doi: 10.5194/cp-8-251-2012

Brovkin, V., Ganopolski, A., Archer, D., & Rahmstorf, S. (2007). Lowering of glacial atmospheric CO_2 in response to changes in oceanic circulation and marine biogeochemistry. *Paleoceanography*, *22*(PA4202). doi: 10.1029/2006PA001380

Brovkin, V., Hofmann, M., Bendtsen, J., & Ganopolski, A. (2002). Ocean biology could control atmospheric $\delta^{13}C$ during glacial-interglacial cycle. *Geochem. Geophy. Geosyst.*, *3*(1027). doi: 10.1029/2001GC000270

Buchanan, P. J., Matear, R. J., Lenton, A., Phipps, S. J., Chase, Z., & Etheridge, D. M. (2016). The simulated climate of the Last Glacial Maximum and insights into the global marine carbon cycle. *Clim. Past*, *12*, 2271–2295. doi: 10.5194/cp-12-2271-2016

Eakins, B., & Sharman, G. (2010). *Volumes of the World's Oceans from ETOPO1.* `https://www.ngdc.noaa.gov/mgg/global/etopo1_ocean_volumes.html`. NOAA National Geophysical Data Center, Boulder, CO.

Francois, R., Altabet, M. A., Yu, E.-F., Sigman, D. M., Bacon, M. P., Frankk, M., ... Labeyrie, L. D. (1997). Contribution of Southern Ocean surface-water stratification to low atmospheric CO_2 concentrations during the last glacial period. *Nature*, *389*, 929–935.

Ganopolski, A., Petoukhov, V., Rahmstorf, S., Brovkin, V., Claussen, M., Eliseev, A., & Kubatzki, C. (2001). CLIMBER-2: a climate system model of intermediate complexity. Part II: model sensitivity. *Climate Dynamics*, *17*(10), 735–751. doi: 10.1007/S003820000144

Goosse, H., Brovkin, V., Fichefet, T., Haarsma, R., Huybrechts, P., Jongma, J., ... Weber, S. L. (2010). Description of the Earth system model of intermediate complexity LOVECLIM version 1.2. *Geoscientific Model Development*, *3*(2), 603–633. doi: 10.5194/gmd-3-603-2010

Gottschalk, J., Battaglia, G., Fischer, H., Frölicher, T. L., Jaccard, S. L., Jeltsch-Thömmes, A., ... Thomas F. Stocker, T. F. (2020). Mechanisms of millennial-scale atmospheric CO_2 change in numerical model simulations. *Quaternary Science Reviews*, 30–74. doi: 10.1016/j.quascirev.2019.05.013

Hain, M. P., Sigman, D. M., & Haug, G. H. (2010). Carbon dioxide effects of Antarctic stratification, North Atlantic Intermediate Water formation, and subantarctic nutrient drawdown during the last ice age: Diagnosis and synthesis in a geochemical box model. *Global Biogeochem. Cy.*, *24*(GB4023). doi: 10.1029/2010GB003790

Hajima, T., Watanabe, M., Yamamoto, A., Tatebe, H., Noguchi, M. A., Abe, M., ... Kawamiya, M. (2020). Development of the MIROC-ES2L Earth system model

and the evaluation of biogeochemical processes and feedbacks. *Geosci. Model Dev.*, *13*, 2197–2244. doi: 10.5194/gmd-13-2197-2020

Ilyina, T., Six, K. D., Segschneider, J., Maier-Reimer, E., Li, H., & Núñez Riboni, I. (2013). Global ocean biogeochemistry model HAMOCC: Model architecture and performance as component of the MPI-Earth system model in different CMIP5 experimental realizations. *Journal of Advances in Modeling Earth Systems*, *5*, 287–315. doi: 10.1029/2012MS000178

Ivanovic, R. F., Gregoire, L. J., Kageyama, M., Roche, D. M., Valdes, P. J., Burke, A., ... Tarasov, L. (2016). Transient climate simulations of the deglaciation 21–9 thousand years before present (version 1) PMIP4 Core experiment design and boundary conditions. *Geosci. Model Dev.*, *9*, 2563–2587. doi: 10.5194/gmd-9-2563-2016

Jones, C. D., Arora, V., Friedlingstein, P., Bopp, L., Brovkin, V., Dunne, J., ... Zaehle, S. (2016). C4MIP The Coupled ClimateCarbon Cycle Model Intercomparison Project: experimental protocol for CMIP6. *Geosci. Model Dev.*, *9*, 2853–2880. doi: 10.5194/gmd-9-2853-2016

Kageyama, M., Albani, S., Braconnot, P., Harrison, S. P., Hopcroft, P. O., Ivanovic, R. F., ... Zheng, W. (2017). The PMIP4 contribution to CMIP6 Part 4: Scientific objectives and experimental design of the PMIP4-CMIP6 Last Glacial Maximum experiments and PMIP4 sensitivity experiments. *Geoscientific Model Development*, *10*, 4035–4055. doi: 10.5194/gmd-10-4035-2017

Kageyama, M., Braconnot, P., Harrison, S. P., Haywood, A. M., Jungclaus, J. H., Otto-Bliesner, B. L., ... Zhou, T. (2018). The PMIP4 contribution to CMIP6 Part 1: Overview and over-arching analysis plan. *Geoscientific Model Development*, *11*, 1033–1057. doi: 10.5194/gmd-11-1033-2018

Kageyama, M., Harrison, S. P., Kapsch, M.-L., Löfverström, M., Lora, J. M., Mikolajewicz, U., ... Volodin, E. (2021). The PMIP4-CMIP6 Last Glacial Maximum experiments: preliminary results and comparison with the PMIP3-CMIP5 simulations. *Clim. Past*. doi: 10.5194/cp-2019-169

Kerr, J., Rickaby, R., Yu, J., Elderfield, H., & Sadekov, A. Y. (2017). The effect of ocean alkalinity and carbon transfer on deep-sea carbonate ion concentration during the past five glacial cycles. *Earth and Planetary Science Letters*, *471*, 42–53. doi: 10.1016/j.epsl.2017.04.042

Khatiwala, S., Schmittner, A., & Muglia, J. (2019). Air-sea disequilibrium enhances ocean carbon storage during glacial periods. *Sci. Adv.*, *5*(6). doi: 10.1126/sciadv.aaw4981

Kobayashi, H., & Oka, A. (2018). Response of Atmospheric pCO_2 to Glacial Changes in the Southern Ocean Amplified by Carbonate Compensation. *Paleoceanography and Paleoclimatology*, *33*, 1206–1229. doi: 10.1029/2018PA003360

Kohfeld, K. E., & Ridgwell, A. (2009). In *Surface ocean-lower atmosphere processes, volume 187* (chap. Glacial-interglacial variability in atmospheric CO_2). doi: 10.1029/2008GM000845

Lambeck, K., Rouby, H., Purcell, A., Sun, Y., & Sambridge, M. (2014). Sea level and global ice volumes from the Last Glacial Maximum to the Holocene. *Proceedings of the National Academy of Sciences*, *111*(43), 15296–15303. doi: 10.1073/pnas.1411762111

Lhardy, F., Bouttes, N., Roche, D. M., Crosta, X., Waelbroeck, C., & Paillard, D. (2021). Impact of Southern Ocean surface conditions on deep ocean circulation at the LGM: a model analysis. *Climate of the Past*. doi: 10.5194/cp-2020-148

Liu, B., Six, K. D., & Ilyina, T. (2021). Incorporating the stable carbon isotope ^{13}C in the ocean biogeochemical component of the Max Planck Institute Earth System Model. *Biogeosciences*, *18*, 4389–4429. doi: 10.5194/bg-18-4389-2021

Lüthi, D., Le Floch, M., Bereiter, B., Blunier, T., Barnola, J.-M., Siegenthaler, U., ... Stocker, T. F. (2008). High-resolution carbon dioxide concentration

record 650,000–800,000 years before present. *Nature*, *453*, 379–382. doi: 10.1038/nature06949

Marzocchi, A., & Jansen, M. F. (2019). Global cooling linked to increased glacial carbon storage via changes in Antarctic sea ice. *Nature geoscience*, *12*, 1001-1005. doi: 10.1038/s41561-019-0466-8

Matsumoto, K., & Sarmiento, J. L. (2002). Silicic acid leakage from the Southern Ocean: A possible explanation for glacial atmospheric pCO_2. *Global Biogeochem. Cy.*, *16*(3). doi: 10.1029/2001GB001442

Mauritsen, T., Bader, J., Becker, T., Behrens, J., Bittner, M., Brokopf, R., & et al. (2019). Developments in the MPI-M Earth System Model version 1.2 (MPI-ESM1.2) and its response to increasing CO_2. *Journal of Advances in Modeling Earth Systems*, *11*, 998–1038. doi: 10.1029/2018MS001400

Menviel, L., Joos, F., & Ritz, S. P. (2012). Simulating atmospheric CO_2 , ^{13}C and the marine carbon cycle during the Last Glacial-Interglacial cycle: possible role for a deepening of the mean remineralization depth and an increase in the oceanic nutrient inventory. *Quaternary Science Reviews*, *56*, 46–68. doi: 10.1016/j.quascirev.2012.09.012

Menviel, L., Yu, J., Joos, F., Mouchet, A., Meissner, K. J., & England, M. H. (2017). Poorly ventilated deep ocean at the Last Glacial Maximum inferred from carbon isotopes: A data-model comparison study. *Paleoceanography*, *32*, 2–17. doi: 10.1002/2016PA003024

Morée, A. L., Schwinger, J., Ninnemann, U. S., Jeltsch-Thömmes, A., Bethke, I., & Heinze, C. (2021). Evaluating the biological pump efficiency of the Last Glacial Maximum ocean using $\delta^{13}C$. *Clim. Past*, *17*, 753–774. doi: 10.5194/cp-17-753-2021

Muglia, J., Somes, C. J., Nickelsen, L., & Schmittner, A. (2017). Combined Effects of Atmospheric and Seafloor Iron Fluxes to the Glacial Ocean. *Paleoceanography*, *32*. doi: 10.1002/2016PA003077

Ödalen, M., Nycander, J., Oliver, K. I. C., Brodeau, L., & Ridgwell, A. (2018). The influence of the ocean circulation state on ocean carbon storage and CO_2 drawdown potential in an Earth system model. *Biogeosciences*, *15*, 1367–1393. doi: 10.5194/bg-15-1367-2018

Ohgaito, R., Yamamoto, A., Hajima, T., Oishi, R., Abe, M., Tatebe, H., ... Kawamiya, M. (2021). PMIP4 experiments using MIROC-ES2L Earth system model. *Geosci. Model Dev.*, *14*, 1195–1217. doi: 10.5194/gmd-14-1195-2021

Oka, A., AbeOuchi, A., Chikamoto, M. O., & Ide, T. (2011). Mechanisms controlling export production at the LGM: Effects of changes in oceanic physical fields and atmospheric dust deposition. *Global Biogeochem. Cy.*, *25*(GB2009). doi: 10.1029/2009GB003628

Otto-Bliesner, B. L., Hewitt, C. D., Marchitto, T. M., Brady, E., Abe-Ouchi, A., Crucifix, M., ... Weber, S. L. (2007). Last Glacial Maximum ocean thermohaline circulation: PMIP2 model intercomparisons and data constraints. *Geophys. Res. Lett.*, *34*(12), 1–6. doi: 10.1029/2007GL029475

Peltier, W. R. (2004). Global glacial isostasy and the surface of the ice-age Earth: the ICE-5G (VM2) model and GRACE. *Annual Review of Earth and Planetary Sciences*, *32*, 111–149. doi: 10.1146/annurev.earth.32.082503.144359

Peltier, W. R., Argus, D. F., & Drummond, R. (2015). Space geodesy constrains ice age terminal deglaciation: The global ICE-6G-C (VM5a) model. *Journal of Geophysical Research - Solid Earth*, *120*, 450–487. doi: 10.1002/2014JB011176

Petoukhov, V., Ganopolski, A., Brovkin, V., Claussen, M., Eliseev, A., Kubatzki, C., & Rahmstorf, S. (2000). CLIMBER-2: a climate system model of intermediate complexity. Part I: model description and performance for present climate. *Climate dynamics*, *16*(1), 1–17. doi: 10.1007/PL00007919

Rickaby, R. E. M., Elderfield, H., Roberts, N., Hillenbrand, C.-D., & Mackensen, A. (2010). Evidence for elevated alkalinity in the glacial Southern Ocean. *Paleoceanography*, *25*(PA1209). doi: 10.1029/2009PA001762

Roche, D. M., Crosta, X., & Renssen, H. (2012). Evaluating Southern Ocean sea-ice for the Last Glacial Maximum and pre-industrial climates: PMIP-2 models and data evidence. *Quat. Sci. Rev.*, *56*, 99–106. doi: 10.1016/j.quascirev.2012.09.020

Roche, D. M., Dokken, T. M., Goosse, H., Renssen, H., & Weber, S. L. (2007). Climate of the Last Glacial Maximum: sensitivity studies and model-data comparison with the LOVECLIM coupled model. *Clim. Past*, *3*(2), 205–224. doi: 10.5194/cpd-2-1105-2006

Schmittner, A., & Galbraith, E. D. (2008). Glacial greenhouse-gas fluctuations controlled by ocean circulation changes. *Nature*. doi: 10.1038/nature07531

Sigman, D. M., & Boyle, E. A. (2000). Glacial/interglacial variations in atmospheric carbon dioxide. *Nature*, *407*, 859–869. doi: 10.1038/35038000

Sigman, D. M., Hain, M. P., & Haug, G. H. (2010). The polar ocean and glacial cycles in atmospheric CO_2 concentration. *Nature*, *466*, 47–55. doi: 10.1038/nature09149

Six, K. D., & Maier-Reimer, E. (1996). Effects of plankton dynamics on seasonal carbon fluxes in an ocean general circulation model. *Global Biogeochem. Cy.*, *10*, 559–583.

Skinner, L. C. (2009). Glacial-interglacial atmospheric CO_2 change: a possible standing volume effect on deep-ocean carbon sequestration. *Clim. Past*, *5*, 537–550. doi: 10.5194/cp-5-537-2009

Stephens, B. B., & Keeling, R. F. (2000). The influence of Antarctic sea ice on glacial-interglacial CO_2 variations. *Nature*, *404*, 171–174.

Tagliabue, A., Aumont, O., & Bopp, L. (2014). The impact of different external sources of iron on the global carbon cycle. *Geophys. Res. Lett.*, *41*, 920–926. doi: 10.1002/2013GL059059

Tagliabue, A., Bopp, L., Roche, D. M., Bouttes, N., Dutay, J.-C., Alkama, R., ... Paillard, D. (2009). Quantifying the roles of ocean circulation and biogeochemistry in governing ocean carbon-13 and atmospheric carbon dioxide at the last glacial maximum. *Clim. Past*, *5*, 695–706. doi: 10.5194/cp-5-695-2009

Watson, A. J., Vallis, G. K., & Nikurashin, M. (2015). Southern Ocean buoyancy forcing of ocean ventilation and glacial atmospheric CO_2. *Nature geoscience*. doi: 10.1038/NGEO2538

Yamamoto, A., Abe-Ouchi, A., Ohgaito, R., Ito, A., & Akira Oka, A. (2019). Glacial CO_2 decrease and deep-water deoxygenation by iron fertilization from glaciogenic dust. *Clim. Past*, *15*(3), 981–996. doi: 10.5194/cp-15-981-2019

Yamamoto, A., Abe-Ouchi, A., & Yamanaka, Y. (2018). Long-term response of oceanic carbon uptake to global warming via physical and biological pumps. *Biogeosciences*, *15*, 4163–4180. doi: 10.5194/bg-15-4163-2018